Nonresonant capture of low-energy protons by ^{27}Al

G. Hardie
Physics Department, Western Michigan University, Kalamazoo, Michigan 49008

R. E. Segel
*Physics Department, Northwestern University, Evanston, Illinois 60201**
and Physics Division, Argonne National Laboratory, Argonne, Illinois 60439

A. J. Elwyn
Fermi National Accelerator Laboratory, Batavia, Illinois 60510

J. E. Monahan
Physics Division, Argonne National Laboratory, Argonne, Illinois 60439
(Received 3 August 1988)

Excitation functions for the ^{27}Al$(p,\gamma)^{28}$Si reaction have been obtained over the energy range $E_p = 0.5-1.8$ MeV. Capture was studied to the ground state (0^+) and the first excited state (2^+) at $E_x = 1779$ keV. Detailed angular distributions were obtained in the energy region near $E_p = 850$, 1060, 1140, and 1623 keV. The data are compared with direct capture calculations which employ a real Woods-Saxon well in both the entrance channel and the final state. The analysis of the data provides no evidence for the presence of a significant semidirect contribution.

I. INTRODUCTION

The resonant capture of particles by nuclei has been investigated for over 50 years and now has a successful theoretical framework. More recently a nonresonant process, the direct capture of a particle by a nucleus, has been the subject of intensive investigation. In this single-step process a compound nucleus is not formed but rather a particle is captured directly into a nuclear orbit with the emission of a gamma ray. From the viewpoint of nuclear spectroscopy the fact that the transition from the initial to the final state proceeds via the electromagnetic interaction rather than the stronger and less-well-known nuclear interaction, offers hope that direct-capture measurements would yield spectroscopic factors more reliable than those obtained from stripping or pickup reactions. An extensive discussion of the extraction of spectroscopic factors from direct-capture studies is given by Rolfs.[1] To assess the accuracy of these spectroscopic factors it is necessary to explore the validity of models used to calculate the direct-capture cross section. In addition, since direct capture is a vital component of astrophysical calculations (see, for example, the review article by Rolfs and Trautvetter[2]) it is important to understand the applicability and limitations of models for this process. A simple model which uses a real square well for the bound state and hard sphere, and Coulomb phase shifts for the initial-state radial wave function has been successful in reproducing the measured nonresonant capture of low-energy protons by light, even-even nuclei (as examples, see Wiescher *et al.*[3] and Rolfs *et al.*[4]). These early successes were followed by additional experimental investigations in which the same model was used to calculate the direct-capture cross sections. In particular some odd-A targets, such as[5] ^{21}Ne and[6] ^{7}Be, were studied because of their astrophysical significance. Recently, heavier nuclei, such as[7] ^{28}Si and[8] ^{40}Ca have been used as targets in direct-capture studies. As the excitation energy is raised, another nonresonant process, semidirect capture,[9,10] becomes important and eventually is much more probable than direct-capture. In the semidirect process the capture proceeds through the excitation of collective modes of oscillation of the nucleus; in particular, the giant dipole resonance.

The high Q value of the ^{27}Al$(p,\gamma)^{28}$Si reaction (11 586 keV) makes accessible with protons from a low-energy, high-current accelerator an energy region in which both the direct and semidirect processes might make contributions to the nonresonant capture. Indeed, a substantial semidirect contribution to the cross section for this reaction has been reported[11] at an incident proton energy (E_p) of 1625 keV. Extensive investigations of the location of ^{27}Al+proton resonances[12,13] have been made, permitting energies for the study of nonresonant capture to be selected between resonances. However, the large number of (p,γ) resonances in the energy region of interest ($E_p = 500$ to 1800 keV) makes it difficult to observe nonresonant capture. Even though these resonances are narrow,[12,13] the cross section at any proton energy will contain contributions from their tails and energies must be found at which these components are smaller than that from nonresonant capture. Indeed, preliminary calculations indicated that there are only a few energies at which this is likely to occur.

Outlined in Sec. II is the procedure used that makes it possible to measure the very small cross sections. In Sec.

III the cross sections are presented, the model used to predict the nonresonant cross sections is given, and the uncertainties associated with the model are noted. Finally, in Sec. IV, the predicted cross sections are compared with those measured and conclusions are drawn.

II. EXPERIMENTAL PROCEDURE

Several aspects of the present experiment render difficult the accurate determination of nonresonant cross sections. At low energies the cross sections are very small (nanobarns) and hence a large amount of beam charge must be accumulated before the nonresonant peak contains a sufficient number of counts and the background can be accurately subtracted. Therefore, the target must maintain its integrity when subjected to beam currents of hundreds of microamperes for many hours. The large number of closely spaced resonances presents another serious problem. Regardless of the energy selected at which to study direct capture, the tails of these resonances will add to the measured cross section and, in fact, may be the dominant contribution even when many half-widths away from the nearest resonance. In addition, beam straggling in the target may result in a peak in the gamma-ray spectrum due to a lower-energy resonance which is near to the nonresonant peak of interest. Reactions with contaminants in the target or target backing may also yield gamma-ray lines close to the one of interest. These considerations dictate the selection of Ge(Li) detectors rather than the much more efficient NaI(Tl) crystals since the energy resolution of the former is much superior to that of the latter.

The large beam currents needed (up to 320 μA was used) in the proton energy range 550–1785 keV were provided by the 4.5 MV Dynamitron accelerator at the Argonne National Laboratory. The targets first used were made by evaporating Al onto the inside of a thin Ta cup. In an attempt to improve heat dissipation later, target backings were made of Cu onto which about 10 mg/cm^2 of Au was electroplated and then onto which the Al was evaporated. Since Cu has a rather low Coulomb barrier and contains low-Z impurities, the purpose of the Au was to reduce the possibility of the production of background gamma radiation by reducing the energy of the protons before they reached the Cu. Targets with thicknesses ranging from 50 to 120 μg/cm^2 were employed. For both types of targets, air or water cooling was used and the holders were mechanically wobbled to spread the deposited energy over a larger area. The target chambers were isolated from ground so that the beam current could be integrated. To prevent build up of C on the target the beam passed through a Ni plated Cu tube kept at liquid-nitrogen temperature. This tube was also isolated from ground and held at a potential of -300 V to suppress electrons ejected from the target. Target thicknesses were measured by going over the ^{27}Al $(p,\gamma)^{28}$Si resonance at $E_p = 991.9$ keV which has a total width of 0.10 keV.[13] This resonance was also used to calibrate the generating voltmeter of the accelerator. The thickness of the target was checked periodically. Provision was made to automatically interrupt the beam in the event of a failure of the target-cooling system.

The gamma rays were detected by three Ge(Li) crystals, each with an active volume of about 80 cm^3 and energy resolution of 7.0$\rightarrow$10.0 keV at a gamma-ray of 6130 keV. In various experimental runs data were collected at angles of 0, 20, 55, 90, 118, and 129 deg: data were not taken at all angles at all energies. For angles $\leq 90°$ the crystals were about 6 cm from the beam spot on the target while at back angles the distances were up to 10.3 cm. Lead discs of thickness 0.32 cm were placed in front of each detector to filter low-energy gamma rays.

Efficiency curves for the detectors, up to a gamma-ray energy of 10 763 keV, were obtained by using the ^{27}Al$(p,\gamma)^{28}$Si resonance at $E_p = 991.9$ keV since the decay scheme of the level formed had been carefully studied[14] and the resonance strength known.[15] For energies above 10 763 keV the efficiencies obtained on the 991.9 keV resonance were extrapolated guided by the shapes of the relative efficiency curves obtained using gamma rays from the resonance at $E_p = 774$ keV. The 774 keV resonance has a strong ground-state transition ($E_\gamma = 12\,331$ keV) but its absolute strength has not been accurately determined.

The signals from the detectors were amplified, digitized, and routed to a PDP11/45 computer. Because it took over 24 h to obtain some of the spectra, care was taken to select very stable electronics. Runs were interrupted about every 2 h to store the spectra on magnetic tape so that it could later be verified that there were no energy shifts and that the target did not deteriorate.

To calculate cross sections the gamma-ray peaks must be correctly identified and their areas determined. An example of the spectra obtained is given in Fig. 1. Gamma lines from direct-capture transitions to several states in ^{28}Si are clearly evident. In addition, there are several prominent peaks due to the presence of contaminants. As this work is concerned with nonresonant capture to the first-excited and ground states, the many lines at low energies are of no consequence. Figure 2 shows a small region of a spectrum in which a primary direct-capture line is expected. Shown are only the single-escape peaks, although the full energies of the gamma rays are quoted. At the bottom of the figure is the gamma-ray populating the first-excited state in ^{28}Si from the resonance at

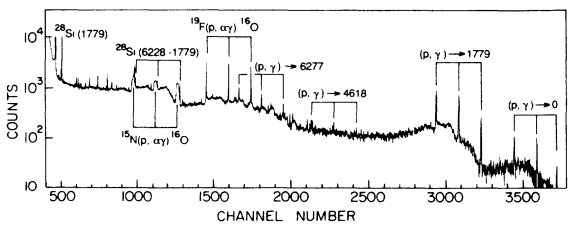

FIG. 1. Pulse height spectrum obtained with 1623 keV protons. The 80 cm^3 detector was at an angle of 55° with respect to the beam direction and 6.4 cm from the beam spot on the target. A total charge of 0.24 C was collected. The lines originating from direct capture to various excited states in ^{28}Si are indicated. All energies are quoted in keV.

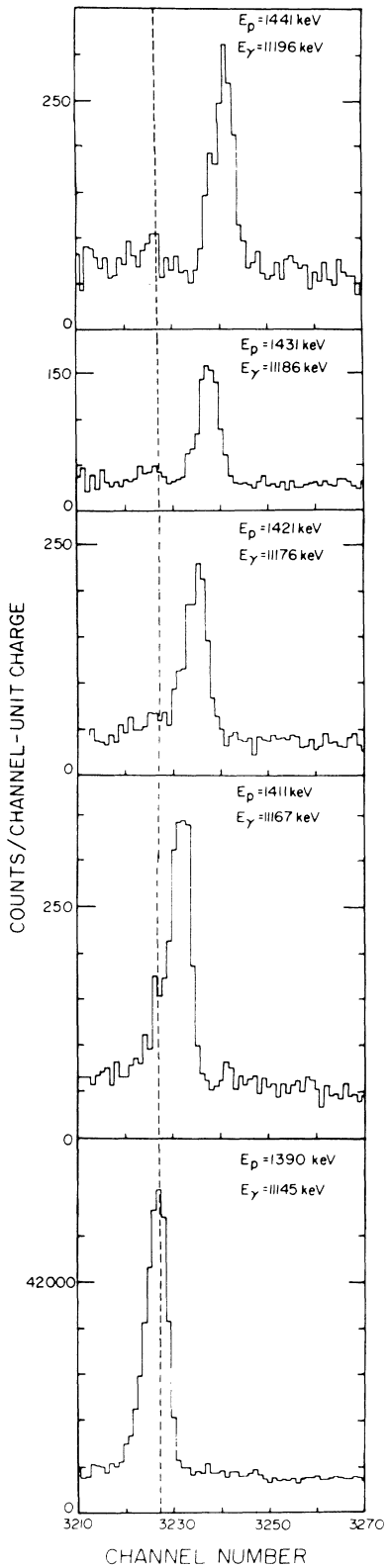

FIG. 2. Pulse height spectrum at 90° as a function of proton energy, near the resonance at $E_p = 1388$ keV. Shown is the first-escape peak but the full energy of the gamma rays is quoted. A total charge of 0.20 C was collected. Although the integrated charge was actually much less for the bottom spectrum, its scale was multiplied to compensate for this. The dashed line is at the energy of the resonance capture peak.

$E_p = 1388$ keV. For strong resonances a resonance peak could be seen as much as 50 keV above the nominal resonance energy. As the beam energy is raised the direct-capture peak become visible. This peak shifts with a change in the incident energy as is evident in the figure. It is clear that at $E_p = 1431$ keV there is no significant contribution to the direct-capture peak from any resonance peak. At lower proton energies the nonresonant capture cross sections are much smaller and the determination of the areas under the peaks correspondingly more difficult.

III. RESULTS AND ANALYSIS

A. Results

The most complete data were for capture into the 1779 keV first excited state in ^{28}Si. Four separate runs were taken and the results to this state are given in Table I. The proton energies, quoted to the front of the target, have an uncertainty of about ± 1 keV. When a data point was repeated an average weighted by the uncertainty is given.

The data were analyzed in terms of Legendre polynomials, $(d\sigma/d\omega) = \sum_n a_n P_n(\cos\theta)$, and therefore $\sigma(E) = 4\pi a_0$. The values for σ thus obtained for the transition to the 1779 keV state are plotted in Fig. 3. It can be seen that the cross sections varied by several orders of magnitude depending upon whether data were taken on or off resonance.

The cross sections in Fig. 3, and elsewhere in this paper, are averages over the ≈ 10 keV energy spread caused by the slowing down of the beam in the target. The yield on a resonance much narrower than the target thickness is independent of the target thickness and is given by

$$Y = (\pi/2)\sigma_0 \Gamma/\varepsilon \ ,$$

where σ_0 represents the peak cross section, Γ the resonance width, and ε the stopping power. Thus the average cross sections on resonance are inversely proportional to the target thickness and the different average cross sections that were obtained on various resonances from time to time merely reflect the fact that targets of different thicknesses were used. The main reasons for taking data on resonances were to calibrate the efficiencies of the detectors and to obtain angular distributions.

Also shown in Fig. 3 is the expected cross section from the known resonances.[12] The yield from these resonances was assumed to be an incoherent sum of contributions, each following the Breit-Wigner formula,

$$\sigma = \{(2J_R+1)/[(2J_p+1)(2J_T+1)]\}$$

$$\times(\pi\lambda^2)\{\Gamma_p\Gamma_\gamma/[(E-E_0)^2+(\Gamma/2)^2]\} \ .$$

Here J_R, J_p, and J_T are the spins of the resonance, proton, and target, respectively; Γ_p and Γ_γ are partial widths for proton and gamma decay, respectively, and E_0 is the energy of the resonance. The proton width was assumed to be proportional to the penetrability

TABLE I. Differential cross sections (μb/sr) for the transition to the 2^+ state at $E_x = 1779$ keV. The energy (laboratory) is for protons at the front of the target.

E_p (keV)	0°	20°	55°	90°	118°	129°
550		$(2.10\pm0.85)\times10^{-4}$	$(5.0\pm1.3)\times10^{-4}$			$(4.5\pm1.7)\times10^{-4}$
585		$(3.59\pm0.81)\times10^{-4}$		$(8.3\pm1.4)\times10^{-4}$	$(5.5\pm1.1)\times10^{-4}$	
720	$(1.50\pm0.30)\times10^{-3}$	$(1.76\pm0.31)\times10^{-3}$		$(2.32+0.28)\times10^{-3}$	$(2.60\pm0.33)\times10^{-3}$	
818	$(0.97\pm0.22)\times10^{-3}$	$(1.17\pm0.21)\times10^{-3}$		$(2.56\pm0.30)\times10^{-3}$	$(2.16\pm0.27)\times10^{-3}$	
850	$(0.99\pm0.21)\times10^{-3}$	$(2.14\pm0.33)\times10^{-3}$	$(4.24\pm0.59\times10^{-3}$	$(4.41\pm0.53)\times10^{-3}$	$(3.08\pm0.73)\times10^{-3}$	$(3.34\pm0.62)\times10^{-3}$
969		$(1.35\pm0.29)\times10^{-2}$	$(1.78+0.36)\times10^{-2}$	$(2.60+0.49)\times10^{-2}$		
1027		3.58 ± 0.61	3.54 ± 0.61	$3.28+0.56$		
1050		$(0.92\pm0.21)\times10^{-2}$	$(1.60\pm0.32)\times10^{-2}$	$(2.04\pm0.38)\times10^{-2}$		
1060	$(1.01+0.18)\times10^{-2}$	$(1.00\pm0.13)\times10^{-2}$	$(1.87\pm0.24)\times10^{-2}$	$(2.16\pm0.22)\times10^{-2}$	$(1.77\pm0.31)\times10^{-2}$	$(1.91+0.34)\times10^{-2}$
1131		$(1.35\pm0.30)\times10^{-2}$	$(2.91\pm0.57)\times10^{-2}$	$(3.69\pm0.69)\times10^{-2}$		
1140	$(1.62+0.30)\times10^{-2}$	$(1.91+0.19)\times10^{-2}$	$(3.15\pm0.39)\times10^{-2}$	$(4.20+0.36)\times10^{-2}$	$(3.36+0.39)\times10^{-2}$	$(3.19\pm0.53)\times10^{-2}$
1155		$(2.53+0.31)\times10^{-2}$	$(5.00\pm0.90)\times10^{-2}$	$(5.72\pm0.66)\times10^{-2}$	$(5.30\pm0.73)\times10^{-2}$	
1234		$(1.10+0.15)\times10^{-1}$	$(0.96\pm0.17)\times10^{-1}$	$(0.81\pm0.14)\times10^{-1}$		
1245	$(1.05\pm0.17)\times10^{-1}$	$(0.95\pm0.16)\times10^{-1}$	$(0.87\pm0.11)\times10^{-1}$	$(0.83\pm0.14)\times10^{-1}$	$(0.72\pm0.12)\times10^{-1}$	$(0.83\pm0.13)\times10^{-1}$
1257		$(1.66\pm0.29)\times10^{-1}$	$(1.44+0.20)\times10^{-1}$	$(1.07\pm0.15)\times10^{-1}$		
1421		$(3.70+0.63)\times10^{-1}$	$(4.04\pm0.70)\times10^{-1}$	$(4.57\pm0.79)\times10^{-1}$		
1431	$(2.40\pm36)\times10^{-1}$	$(2.35\pm0.33)\times10^{-1}$	$(3.00\pm0.42)\times10^{-1}$	$(3.15\pm0.44)\times10^{-1}$	$(2.80\pm0.43)\times10^{-1}$	
1441		$(2.10\pm0.37)\times10^{-1}$	$(2.58+0.36)\times10^{-1}$	$(2.55\pm0.36)\times10^{-1}$		
1613		$(0.81\pm0.14)\times10^{-1}$	$(1.21\pm0.21)\times10^{-1}1$	$(1.41\pm0.24)\times10^{-1}$		
1623	$(0.99\pm0.17)\times10^{-1}$	$(0.94\pm0.12)\times10^{-1}$	$(1.53\pm0.15)\times10^{-1}$	$(1.65+0.14)\times10^{-1}$	$(1.54\pm0.27)\times10^{-1}$	$(1.73\pm0.29)\times10^{-1}$
1633		$(1.49\pm0.27)\times10^{-1}$	$(1.91+0.34)\times10^{-1}$	$(2.25+0.40)\times10^{-1}$		
1643		$(2.15\pm0.38)\times10^{-1}$	$(2.94\pm0.51)\times10^{-1}$	$(3.03\pm0.52)\times10^{-1}$		
1653		$(6.8+1.2)\times10^{-1}$	$(8.0\pm1.4)\times10^{-1}$	$(7.3+1.3)\times10^{-1}$		
1785		$(1.41\pm0.25)\times10^{-1}$	$(1.80\pm0.31)\times10^{-1}$	$(1.63\pm0.28)\times10^{-1}$		

$$P_l = (G_l^2 + F_l^2)^{-1} kr$$

in which F_l and G_l represent, respectively, the regular and irregular solutions of the extra-nuclear radial equation for collisions with orbital angular momentum l. In the formula for σ it should be noted that at energies more than a few half-widths away from a resonance it is the $(E - E_0)^2$ term which dominates the denominator and therefore the yield varies much more slowly with energy than it does near the resonance. Thus the resonant capture can overwhelm the very small nonresonant capture even at energies many half-widths away from any resonance.

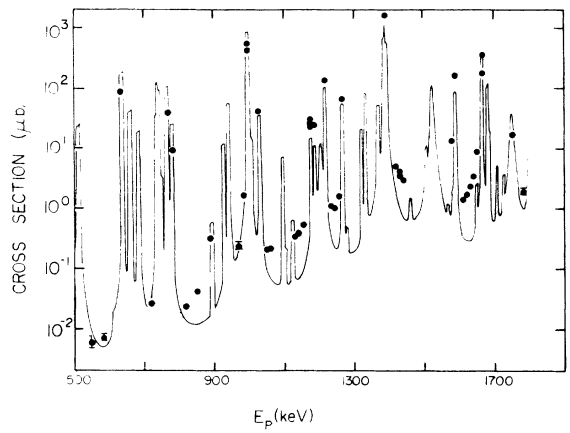

FIG. 3. Cross sections for populating the first-excited state in ^{28}Si. Unless indicated by error bars, the uncertainties are comparable to, or smaller than, the size of the dots. The solid curve is the cross section obtained by the incoherent addition of the known resonances (see Sec. III A).

It can be seen from Fig. 3 that at energies well removed from resonances the observed yield for capture to the first-excited state of ^{28}Si is up to an order of magnitude greater than that calculated from the known resonances. This suggests a nonresonant capture component which becomes prominent when the resonance yield is sufficiently small. It should be noted that in the lower portion of the energy region covered in the present work, only upper limits have been established[12] for the proton widths of a number of the resonances, and these upper limits have been used in estimating the yield. Thus the calculated yield in the low-energy region of Fig. 3 is an upper limit.

The angular distributions provide further evidence for a prominent nonresonant capture component. Angular distributions at four energies away from resonances are shown in Fig. 4 and three distributions on resonances are shown in Fig. 5. The difference between the two sets of data is striking. In each case the yield on resonance is isotropic to within about 10% while, for the off-resonance distributions, the cross section at 90° is a factor of 2 or more greater than that at 0°. The ratio of the coefficients a_2/a_0 in the Legendre polynomial expansion is plotted as a function of proton energy in Fig. 6. Comparing this figure with Fig. 3, it is clear that while a_2/a_0 is near zero over most of the range, it often becomes large

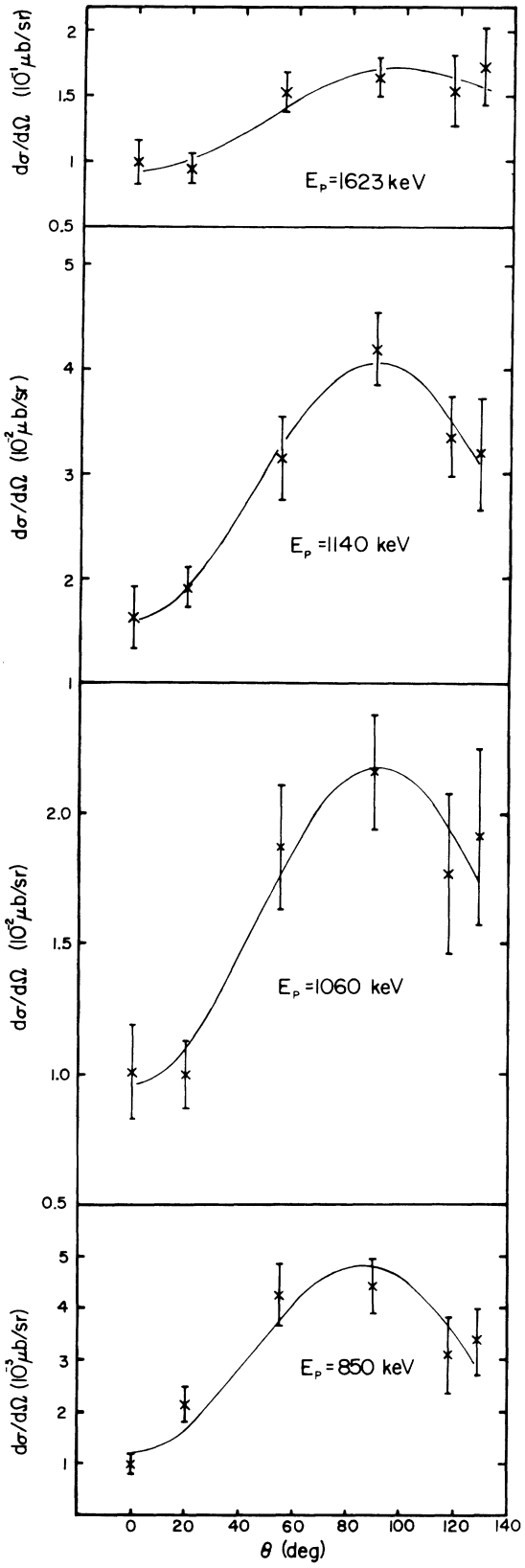

FIG. 4. Examples of angular distributions at incident proton energies selected to be between compound nucleus resonances. The cross sections are for populating the first-excited state in ^{28}Si. The curves are Legendre polynomial fits.

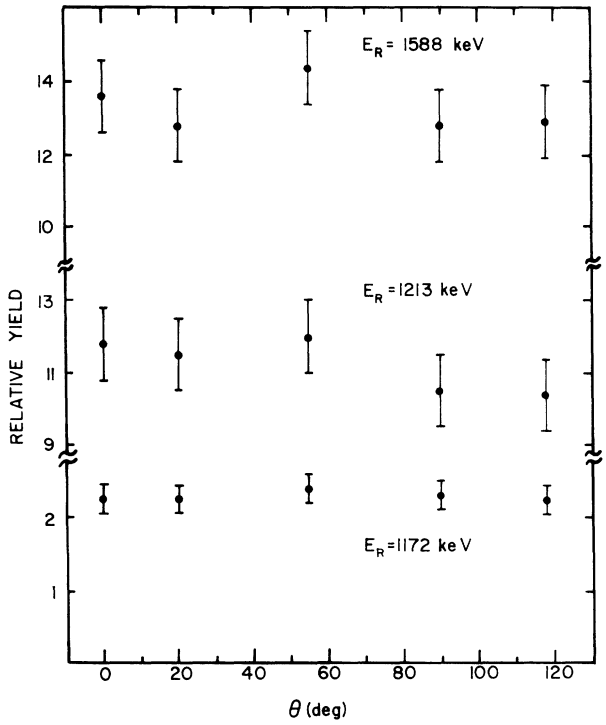

FIG. 5. Examples of angular distributions on resonances.

and negative in regions away from resonances where the observed yield is larger than that predicted from the known resonances. Thus there appears to be an underlying nonresonant capture whose angular distribution is approximated by $[1-0.5P_2(\cos\theta)]$.

The capture cross sections to the ground state are about a factor of 5 lower than those to the first-excited state, as might be expected from the lower spin of the ground state. Therefore, considerably less data were obtained for the ground-state transition. The cross sections that were obtained at various energies are listed in Table II and are shown in Fig. 7, along with the yield calculated

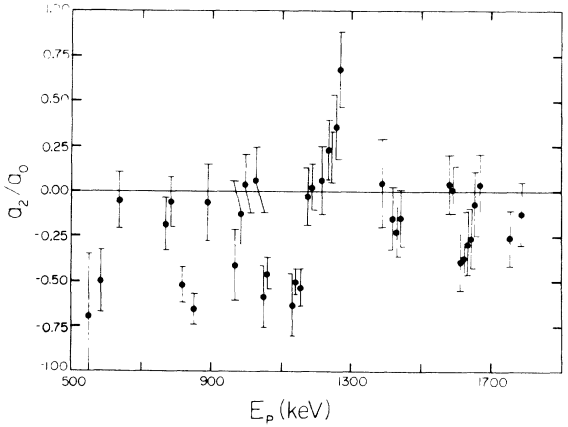

FIG. 6. The ratio of the coefficients in the Legendre polynomial fits to the data for the transition to the first-excited state in ^{28}Si.

TABLE II. Differential cross sections (μb/sr) for the transition to the 0^+ ground state. The energy (laboratory) is for protons at the front of the target.

E_p (keV)	0°	20°	55°	90°	118°	129°
818	$(8.4\pm1.7)\times10^{-4}$			$(7.9\pm1.7)\times10^{-4}$	$(6.5\pm1.7)\times10^{-4}$	
850	$(9.2+1.8)\times10^{-4}$	$(7.6+1.7)\times10^{-4}$	$(8.9\pm1.7)\times10^{-4}$	$(8.4\pm1.3)\times10^{-4}$	$(6.8\pm1.7)\times10^{-4}$	$(7.6\pm1.6)\times10^{-4}$
1060	$(3.92+0.67)\times10^{-3}$			$(3.09\pm0.55)\times10^{-3}$	$(2.83\pm0.50)\times10^{-3}$	
1140	$(4.45\pm0.86)\times10^{-3}$	$(4.05\pm0.54)\times10^{-3}$	$(4.56\pm0.86)\times10^{-3}$	$(5.7\pm0.6)\times10^{-3}$	$(7.1\pm0.9\times10^{-3}$	$(7.0\pm1.3)\times10^{-3}$
1188		4.72±0.77	4.00±0.46	4.65±0.76		3.95±0.64
1245	$(1.08\pm0.17)\times10^{-2}$	$(1.01\pm0.19)\times10^{-2}$	$(0.92\pm0.12)\times10^{-2}$	$(0.67\pm0.09)\times10^{-2}$	$(0.61\pm0.10)\times10^{-2}$	$(0.65+0.12)\times10^{-2}$
1431	$(1.04\pm0.17)\times10^{-2}$			$(0.81\pm0.13)\times10^{-2}$	$(0.494\pm0.088)\times10^{-2}$	
1623	$(3.22\pm0.50)\times10^{-2}$	$(2.88\pm0.39)\times10^{-2}$	$(2.55\pm0.30)\times10^{-2}$	$(2.41\pm0.26)\times10^{-2}$	$(2.17\pm0.35)\times10^{-2}$	$(2.32\pm0.44)\times10^{-2}$
1785		$(7.8\pm1.4)\times10^{-2}$	$(4.86\pm0.86)\times10^{-2}$	$(5.6\pm1.0)\times10^{-2}$		

from the known resonances. Away from resonances the observed cross section is as much as an order of magnitude greater than that estimated for resonant capture. The angular distributions off resonance were close to isotropic and not greatly different from those obtained on the various resonances. Examples are shown in Fig. 8.

Kicinska-Habior *et al.*[11] have reported measurements of the ^{27}Al$(p,\gamma)^{28}$Si reaction at 1625 keV. For both the ground-state and the first-excited state transitions the cross sections found in the present work are about a factor of 2.5 less than those given in Ref. 11. Since few experimental details are given in Ref. 11, it is not possible to locate the source of this discrepancy. Nevertheless, we are confident that the cross sections quoted in the present work are correct to within the stated errors.

B. Direct-capture calculations

Several different approaches have been taken to calculate direct-capture cross sections. Various authors (see, for example, Refs. 3, 4, 7, and 8), following the work of Rolfs,[1] have used a square well for the bound state and hard-sphere phase shifts for the entrance channel. These phase shifts are determined at a rather large value of R, the value being chosen to account for the rounding of the Coulomb and angular momentum barriers by the diffuse edge of the optical potential.[16] This method excludes any contribution to the overlap integral from the nuclear interior. Other investigators (see, for example, Ref. 6) have used Woods-Saxon potentials, which give distorted waves of significant amplitude in the nuclear interior where the bound-state wave function is large and this can result in a significantly larger cross section. In the present work the potential in both the entrance channel and for the bound state was taken to be a real Woods-Saxon well. The radius and diffuseness parameters were the same for both wells. For the bound state, the depth of the well was varied in order to obtain the correct binding energy for the captured proton. In order to investigate the effect of the well shape and parameters on the direct capture cross

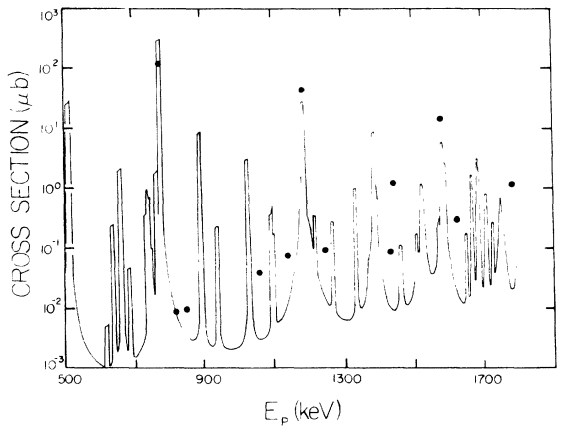

FIG. 7. Cross sections for populating the ground state in ^{28}Si. The uncertainties are comparable to, or smaller than, the size of the dots. The solid curve is the cross section obtained by the incoherent addition of the known resonances for the transition to the first excited state in ^{28}Si (see Sec. III A).

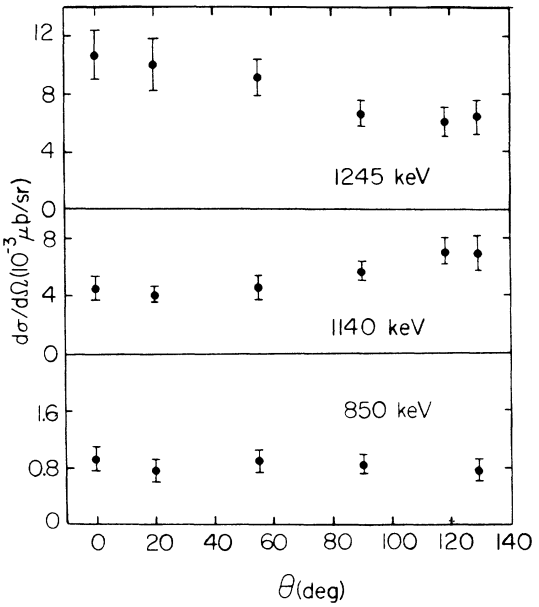

FIG. 8. Examples of angular distributions at incident proton energies selected to be between compound nucleus resonances. The cross sections are for populating the ground state of ^{28}Si.

sections a series of calculations were performed for capture into the $2s$ orbital to form the 1779 keV, 2^+ first-excited state of ^{28}Si. The code HIKARI (Ref. 17) was used and the calculations were performed for an incident bombarding energy of 1623 keV.

In one set of calculations the incident potential was taken to be (a) a high barrier, which is equivalent to a hard sphere, (b) zero (i.e., no well), and (c) attractive with a depth taken from global optical model fits.[18] The radius and diffuseness parameters used were $R_0=1.25$ fm and $a=0.65$ fm.[18] The wave function for an $l=1$ distorted wave for these three cases is shown in Fig. 9. The real part of the bound-state eigenfunction is also plotted in the figure. The resulting total cross sections are 0.608 μb (barrier), 1.52 μb (no well in entrance channel), and 6.79 μb (Woods-Saxon well). The calculated cross sections are clearly very sensitive to the type of potential used for the incident wave, and, in particular, it is apparent that contributions from the nuclear interior can be very important.

The sensitivity of the cross sections to the well parameters is illustrated in Table III where the effect of varying each parameter (V, R_0, and a) by $\pm 5\%$ from its nominal value is shown. It is apparent from Table III that changes of only a few percent in the parameters can change the cross section by a factor of 2 or more. Another aspect of this sensitivity is shown in Fig. 10 where the cross section as a function of energy is plotted for two values of the radius parameter; $R_0=1.25$ fm and $R_0=1.19$ fm. The marked sensitivity of the cross section to this parameter is clearly evident. This sensitivity decreases as the excitation energy in ^{28}Si increases, as is also shown in Fig. 10, which gives the results for an identical set of calculations except that the excitation energy was increased from 1779 to 9585 keV. Clearly, even for one particular target nucleus, a single number cannot be given to indicate the sensitivity of the cross section to a variation in one of the parameters. The way in which the great sensitivity to the potential parameters occurs becomes clearer when the shape of the calculated yield curves is examined. The calculated yield is dominated by a single resonance, a size resonance, which is severely distorted by penetrability. At energies near to the resonance peak the sensitivity to the well parameters is particularly great. It should be noted that if hard-sphere phase shifts are used in the entrance channel, the size resonance does not appear. The uncertainties associated with the optical-model parameters at the proton energies used in this experiment seriously limit the accuracy of the calculated direct-capture cross sections.

The calculated direct-capture cross sections are shown in Fig. 11 along with the experimental data. Well away from resonances the calculations accurately predict the yield for the excited-state transition while the ground-state yield is overestimated by a factor of 1.5–2 with the ratio of experiment to calculation being greatest at lower energies. In making these calculations the spectroscopic factors from the compilation of Endt[19] were used. The

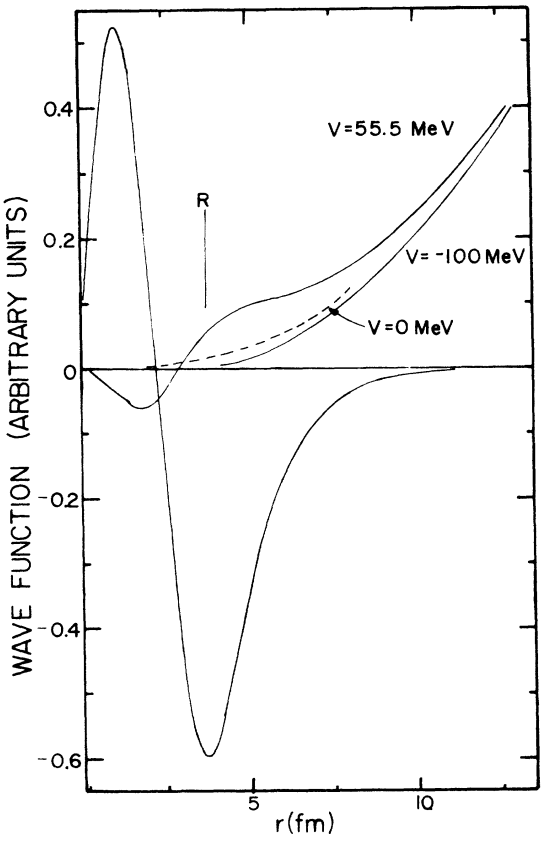

FIG. 9. The wave function for an $l=1$ distorted wave for different specifications of the nuclear force in the entrance channel: an attractive Woods-Saxon well (55.5 MeV), no well ($V=0$ MeV), and a barrier ($V=-100$ MeV). Also plotted is the real part of the bound-state eigenfunction. The symbol R indicates the location of $R_0 A^{1/3}$, with $R_0=1.25$ fm.

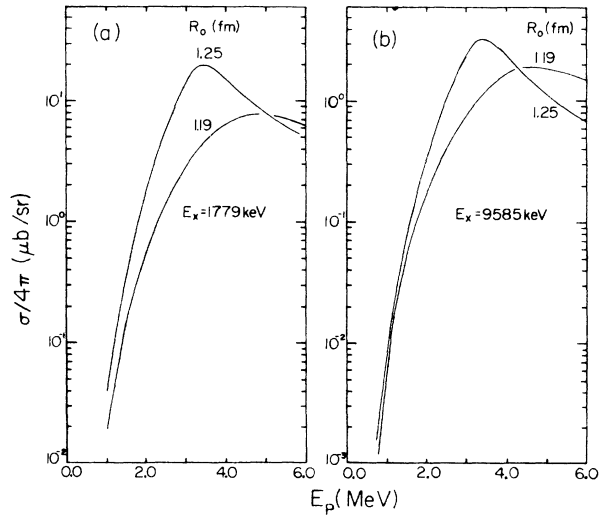

FIG. 10. Excitation functions for the direct capture into the $2s$ orbit for two different radius parameters of $R_0=1.25$ fm and $R_0=1.19$ fm, for the Woods-Saxon well. The two sets of calculations are for two different excitation energies in ^{28}Si.

TABLE III. The sensitivity of the total cross section to a change in the parameters R_0 and a which describe the shape of the Woods-Saxon wells, and to the parameter V which is the depth of the entrance-channel well. Shown is the ratio of the cross section obtained with a changed parameter to that obtained with the standard set. The 1623 keV protons are captured into the $2s$ state and three different final 2^+ states are considered.

E_x (keV)=	1779	7381	9380
R_0 (fm)			
1.19	0.42	0.54	0.62
1.25	1	1	1
1.31	8.9	6.1	4.4
a (fm)			
0.62	0.81	0.85	0.86
0.65	1	1	1
0.68	1.2	1.2	1.2
V (MeV)			
52.38	0.61	0.71	0.77
55.14	1	1	1
57.90	2.3	1.9	1.6

calculations predict the angular distribution for the gamma-ray to the first excited state to be strongly peaked at 90° while the ground-state transition is expected to be close to isotropic. As can be seen in Figs. 4 and 8, in both cases the predicted shapes of the angular distributions are in agreement with experiment. Figure 12 shows calculated and measured differential cross sections at one energy, 850 keV, where direct capture is believed to dominate. Experimentally, the excited state transition is somewhat more isotropic than predicted, while, as noted above, the cross section to the ground state is about 30% less than calculated and a small dip, rather than a slight peak, is present at 90°.

IV. DISCUSSION AND CONCLUSIONS

Because of the difficulty in determining the very small cross sections at the lower bombarding energies (see Tables I and II), many of then were measured at several different times, often with different targets and detectors, to check the reliability of the measurements. The reproducibility was excellent, usually well within the uncertainties assigned to each measurement. At $E_p = 1623$ keV our differential cross sections are about a factor of 2.5 lower than those of Kicinska-Habior *et al.*[11] at $E_p = 1625$

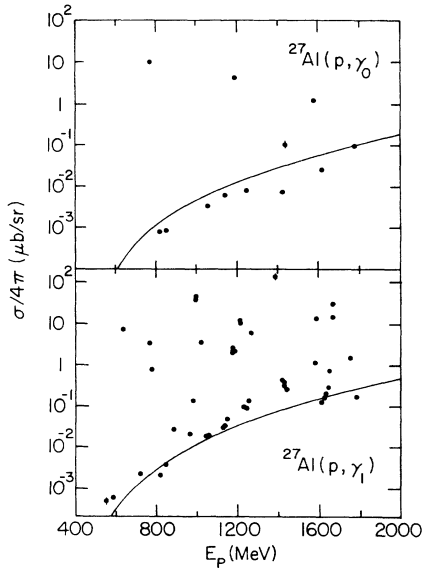

FIG. 11. Experimental and calculated direct capture total cross sections (divided by 4π) for (a) the ground state and (b) the first-excited state transition. The calculation is described in the text.

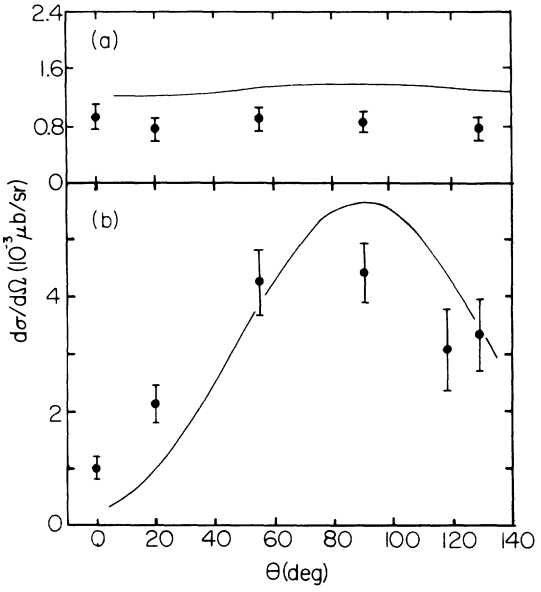

FIG. 12. Experimental and calculated direct capture differential cross sections at an incident proton energy of 850 keV for (a) the ground state and (b) the first-excited state transition.

keV. Although the cross section is changing fairly rapidly in this energy region (see Fig. 3), a discrepancy of this magnitude remains unexplained. As discussed earlier, more extensive angular distribution data for capture to the first-excited state were taken in four proton energy regions (see Fig. 4). These angular distributions are peaked at 90° in sharp contrast to the rather isotropic angular distributions found on resonances. These angular distributions are at least roughly symmetric about 90° and all have large negative values for a_2/a_0. The magnitude of the cross sections as well as the shapes of the angular distributions are in satisfactory agreement with direct-capture calculations. Neither the spectroscopic factors nor the parameters of the direct-capture model were varied in an attempt to improve the fits. It should be noted that changing the two spectroscopic factors involved will change the shape, as well as the magnitude, of the angular distributions. Also, a change in the parameters of the Woods-Saxon wells will not just scale the curve of the cross section as a function of the proton energy, but will also change its shape. Thus, our work provides no evidence for substantial contributions from mechanisms other than direct capture. The opposite conclusion reached by Kicinska-Habior *et al.*[11] is due both to a disagreement regarding the magnitude of the cross sections, and to differences in the direct-capture calculations. In contrast to our calculations (see Sec. III B) they used hard-sphere phase shifts ($R_0=1.3$ fm) in the entrance channel and a real Woods-Saxon potential ($R_0=1.3$ fm) in the final state. As usual, the depth of this potential was chosen to reproduce the binding energy of the captured proton. They do not quote a diffuseness parameter for the Woods-Saxon potential nor do they record the spectroscopic factors used. Their calculation is said to include contributions from the tails of nearby compound-nucleus resonances but no details are given.

The direct-capture calculations also give a satisfactory fit to the ground-state capture well away from resonances. The calculations predict a slight increase in cross section from 0° to 90° while most, but not all, angular distributions are somewhat peaked at 0°. Also, there is some indication of asymmetry about 90°, an effect which could not result from the coherent addition of $E1$ radiation from the direct and semidirect processes, but could be due to contributions from the tails of isolated resonances. A peaking at 0° and an asymmetry about 90° would result from a sufficiently strong $M1$ contribution. However, including an $M1$ amplitude in our program does not result in a contribution of sufficient magnitude to alter significantly the shape of the predicted ground-state angular distribution. The limited amount of data and the rather large experimental uncertainties combined with the lack of knowledge of the parameters of the isolated resonances make it unproductive to attempt a more detailed analysis.

Direct-capture calculations were performed for other nuclei for which data have been reported. The optical model parameters were the same as those used for the ^{27}Al($p\gamma$) calculations and spectroscopic factors were taken from the literature. Results are shown in Fig. 13. For[20] ^{20}Ne and[8] ^{40}Ca the calculation gives a satisfactory fit to the data away from resonances. There also appeared to be satisfactory agreement for[20] ^{24}Mg(p,γ_1) and[7] ^{28}Si(p,γ_0) though in these cases interference between broad resonances and direct capture makes it more difficult to assess how well the calculations reproduce the direct capture component. For[1] ^{16}O(p,γ_1) too little yield is predicted for proton energies below about 1.8 MeV and too much yield at higher incident energies.

The calculations predict strong size resonances in direct capture. For low-A targets these resonances are so broad that they are not discernable but the resonances decrease in energy as A increases while the Coulomb barrier increases as Z increases and, therefore, the resonances become narrower for heavier targets. The calcu-

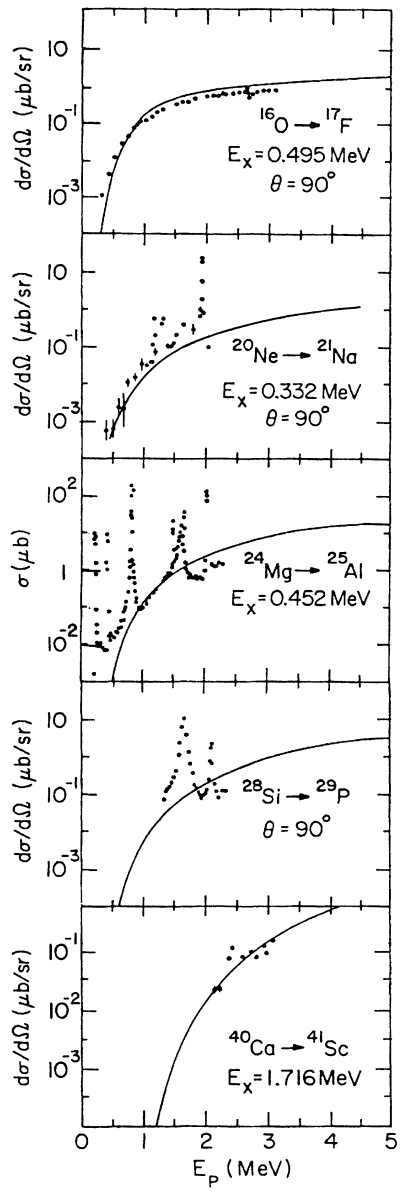

FIG. 13. Experimental and calculated direct-capture cross sections at 90° for various (p,γ) reactions. The ^{16}O data are from Ref. 1, ^{20}Ne and ^{24}Mg from Ref. 20, ^{28}Si from Ref. 7, and ^{40}Ca from Ref. 8.

lations for $^{27}Al(p,\gamma)$ show a p-wave resonance at 3.4 MeV and an f-wave resonance at 6.7 MeV. The cross section in the 0.5 to 2.0 MeV region is dominated by the p-wave resonance and therefore is sensitive to the resonance parameters which, in turn, depend on the optical-model parameters. Thus the calculated cross sections can depend critically on the optical-model parameters as noted in Sec. III. For $^{40}Ca(p,\gamma)$ the lowest size resonance is predicted to be at about 1.4 MeV with a width of about 10 keV.

Overall it is felt that the direct-capture calculations of the present work, in which no attempt was made to vary the parameters to improve the fits, is in satisfactory agreement with all existing low-energy, nonresonant, proton capture data.

ACKNOWLEDGMENTS

We wish to thank Dr. Michael Wiescher of the University of Notre dame for help during the early phase of this work. It is a pleasure to acknowledge many helpful discussions with Dr. Dean Halderson of Western Michigan University. We are grateful to Rozana Hussain, Dave Baran, and Moustafa Saber for aid in collecting the data. We would also like to thank the dynamitron operating staff for their aid and cooperation. Two of us (G.H. and R.E.S.) wish to thank the Argonne National Laboratory for its support and hospitality. This work was supported by the U.S. Department of Energy, Division of Nuclear Physics, under Contract No. W-31-109-ENG-38 and the National Science Foundation (Contract No. PHY8608247).

---

*Permanent address.

[1]C. Rolfs, Nucl. Phys. **A217**, 29 (1973).

[2]C. Rolfs and H. P. Trautvetter, Ann. Rev. Nucl. Sci. **28**, 115 (1978).

[3]M. Wiescher, H. W. Becker, J. Gorres, K. -U. Kettner, H. P. Trautvetter, W. E. Kieser, C. Rolfs, R. E. Azuma, K. P. Jackson, and J. W. Hammer, Nucl. Phys. **A349**, 165 (1980).

[4]C. Rolfs, W. S. Rodney, M. H. Shapiro, and H. Winkler, Nucl. Phys. **A241**, 460 (1975).

[5]J. Gorres, H. W. Becker, L. Buchmann, C. Rolfs, P. Schmalbrock, H. P. Trautvetter, A. Vlieks, J. W. Hammer, and T. R. Donoghue, Nucl. Phys. **A408**, 372 (1983).

[6]K. H. Kim, M. H. Park, and B. T. Kim, Phys. Rev. C **35**, 363 (1987) and references cited therein.

[7]F. Terrasi, A. Brondi, P. Cuzzocrea, R. Moro, and M. Romano, Nucl. Phys. **A324**, 1 (1979).

[8]F. Terrasi, A. Brondi, P. Cuzzocrea, R. Moro, G. LaRana, M. Romano, B. Gonsior, N. Notthoff, and E. Kabuss, Nucl. Phys. **A394**, 405 (1983).

[9]G. E. Brown, Nucl. Phys. **57**, 339 (1964).

[10]C. F. Clement, A. M. Lane, and J. R. Rook, Nucl. Phys. **66**, 273 (1965).

[11]M. Kicinska-Habior, P. Decowski, M. Dabrowska, W. Grochulski, P. Jaracz, T. Matulewicz, B. Sikora, J. Toke, and E. Somorjai, Z. Phys. A **312**, 89 (1983).

[12]P. M. Endt and C. Van Der Leun, Nucl. Phys. **A310**, 1 (1978).

[13]R. O. Nelson, E. G. Bilpuch, C. R. Westerfeldt, and G. E. Mitchell, Phys. Rev. C **29**, 1656 (1984).

[14]A. Anttila, J. Keinonen, M. Hautala, and I. Forsblom, Nucl. Instrum. Methods **147**, 501 (1977).

[15]B. M. Paine and D. G. Sargood, Nucl. Phys. A **331**, 389 (1979).

[16]E. Vogt, C. Michaud, and H. Reeves, Phys. Lett. **19**, 570 (1965).

[17]We thank Professor H. Weller of the Physics Department, Duke University, for supplying us with this code.

[18]C. M. Perey and F. G. Perey, At. Data Nucl. Data Tables **17**, 1 (1976).

[19]P. M. Endt, At. Data Nucl. Data Tables **19**, 23 (1977).

[20]H. P. Trautvetter and C. Rolfs, Nucl. Phys. A **242**, 519 (1975).